JOURNAL OF Materials CHEMISTRY

Electroreductive deposition of polymeric coatings having Ru^{II} redox centers on Pt, Pd and sintered Fe–(5–10)%Ni electrodes

M. M. S. Paula,[a] V. N. de Moraes Jr.,[b] F. Mocellin[b] and C. V. Franco*[b†]

[a]*Depto. de Engenharia de Materiais, Universidade do Extremo Sul Catarinense-UNESC, Av. Universitária, 1105, Criciúma-SC-88806–000, Brazil*

[b]*Departamento de Química, Universidade Federal de Santa Catarina- UFSC,Campus Trindade, Florianópolis, SC-88 040–900, Brazil*

Pt, Pd and sintered Fe–(5–10)%Ni electrodes were coated by reductive electrodeposition of electrochemically generated *trans*-$[RuCl_2(vpy)_4]$-based films (vpy = 4-vinylpyridine). The complex *trans*-$[RuCl_2(vpy)_4]$ was synthesized from a ruthenium blue solution and characterized by various techniques including electronic spectroscopy (446 nm), FTIR, ^1H and ^{13}C NMR elemental analysis and cyclic voltammetry ($E_{1/2} = -103.5$ mV *vs.* $Ag–Ag^+$). The results obtained confirmed the proposed structure of the monomer. Electrochemical studies carried out on films generated by either a potentiostatic or a galvanostatic approach revealed that the redox properties of poly-*trans*-$[RuCl_2(vpy)_4]$ were similar to those of the monomer in solution. The morphology of the films was investigated by scanning electron microscopy (SEM). Microprobe X-ray dispersive energy analysis (EDS) was also performed on the polymer surface. The feasibility of film formation on Fe–5%Ni and Fe–10%Ni sintered electrodes has been demonstrated.

The electrodeposition of polymeric films with redox centers is a promising approach for corrosion protection and electrocatalysis, where low oxidation-state metals added to a polymeric matrix act as sacrificial anodes. Moreover, when applied to a porous substrate, the resulting material can act as a fixed bed catalyzer. Several reports on oxidative electrodeposition of films for corrosion protection of steel substrates can be found in the literature.[1–7] Nevertheless, oxidative electrodeposition shows a drawback when applied to active metals and alloys, as anodic dissolution of the substrate occurs for potential values similar to those required for the electropolymerization reactions. In order to overcome such difficulties, our group has synthesized and characterized a series of novel complexes of general formula *trans*-$[RuCl_2L_4]$, where L is a ligand containing reductively electropolymerizing sites. In an electroreductive process, films are generated in the potential region of cathodic protection of the substrates, which allows for higher stability upon electropolymerization. The present work shows the success of this approach as applied to the case L = 4-vinylpyridine (Fig. 1). The electropolymerization reactions were carried out by either a potentiostatic or galvanostatic approach on inert Pt and Pd electrodes, as well as on Fe–5%Ni and Fe–10%Ni sintered substrates.

Experimental

Reagents

All reagents and solvents employed in this work were of an analytical grade and purchased from a variety of commercial sources. $RuCl_3 \cdot 3H_2O$ (Jonhson-Matthey) and 4-vinylpyridine (Aldrich) were used without further purification. Description of the experimental procedures can be found elsewhere.[8,9]

Synthesis

The general steps followed for the synthesis of *trans*-$[RuCl_2(vpy)_4]$ have been detailed in previous work, as applied to similar complexes.[9,10] A 'ruthenium blue'[11] solution was prepared from 260 mg (1.0 mmol) of $RuCl_3 \cdot 3H_2O$ followed by the addition of 1.0 ml of 4-vinylpyridine (9.5 mmol) and hydroquinone (100 mg). The system was shielded from light in a flow of argon for 40 min. The volume of the solution was halved by rotatory evaporation. The product was extracted from the reaction solution using chloroform. The organic phase was repeatedly rinsed with distilled water in a separation funnel to remove any residues that might have been present. The final product was obtained by evaporation of $CHCl_3$ and was characterized as a reddish amorphous compound. A yield of 43.70% was estimated based on the initial amount of $RuCl_3 \cdot 3H_2O$. This value was an average of five syntheses. Results from CHN elemental analysis were in good agreement with the expected theoretical composition. Anal. Calc. for $C_{28}H_{28}Cl_2N_4Ru$ (%): C, 56.75; H, 4.76; N, 9.45%. Found: C, 56.74; H, 4.92; N, 9.45%.

Spectroscopical and spectroelectrochemical analyses

IR spectra of KBr pellets were obtained on a Perkin-Elmer FTIR model 1 GPC FTIR spectrophotometer and electronic spectra were obtained using a Hewlett Packard model HP8452A spectrophotometer in quartz cuvettes (path length = 1.0 cm). ^1H and ^{13}C NMR data were gathered from a 200 MHz Bruker model AC200F in $CDCl_3$. Both the optically transparent thin layer electrode (OTTLE) and cell have been described in a recent paper.[12]

Electrochemical measurements

Electrochemical measurements were carried out at 23 ± 2 °C using a Princeton Applied Research (PARC) Model 273A

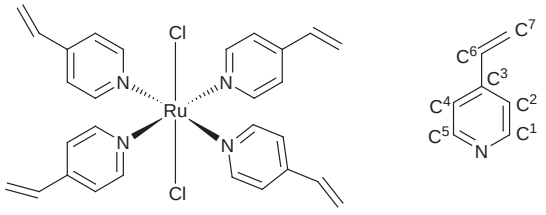

Fig. 1 Proposed structure for the *trans*-$[RuCl_2(vpy)_4]$ complex

†E-mail: franco@labmat.ufsc.br

potentiostat/galvanostat, interfaced with a DOS compatible computer through a National Instrument general purpose interface board (GPIB). Both Pt and Pd discs purchased from EG&G PARC were sealed in a Teflon insulator. The cell and instrumentation setup have recently been thoroughly described in the literature.[8] Films were generated on either a Pt or Pd electrode, previously prepared according to the procedure explained in related work.[13] All electrochemical experiments requiring an inert atmosphere were performed in a conventional three-electrode cell filled with ultra-pure argon (White–Martins). Galvanostatic deposition was carried out in a specially designed cell.[14]

Sintering

Fe–5%Ni and Fe–10%Ni electrodes were sintered from mixtures of elemental powders containing 95%Fe–5%Ni + 0.8% zinc stearate, and 90%Fe–10%Ni + 0.8% zinc stearate (wt.%), respectively. The powder mixtures were pressed in a double action press and sintered at 1200 °C for 2 h in an H_2 atmosphere. The final density of the sintered materials was 7.50 and 7.52 g cm^{-3} for the Fe–5%Ni and Fe–10%Ni alloys, respectively. Subsequently, the electrodes were mechanically polished with gradually finer sandpaper and finished in a 0.25 μm alumina suspension. Further details on the sintering process can be found elsewhere.[15]

Results and Discussion

Synthesis of *trans*-[$RuCl_2(vpy)_4$]

Wilkinson and coworkers[16] pointed out that the syntheses of ruthenium complexes with pyridine-2-thiol and 2-vinylpyridine acting as ligands were not successful. Attempted syntheses resulted in a highly insoluble polymeric diamagnetic species having approximate stoichiometry $[RuCl_2L_2]_n$ and were found to be hard to purify. Conversely, the synthetic approach used in our laboratory has proven to be successful in synthesizing a similar compound $[RuCl_2(vpy)_4]$, in relatively high yield. The key role in the process is apparently played by addition of small amounts of hydroquinone, which possibly acts as a radical inhibitor, preventing both intra- and inter-molecular polymerization of the ligand in the reaction medium. Another complex, *trans*-[$RuCl_2(pmp)_4$][pmp = 3(pyrrol-1-ylmethyl)-pyridine], has been recently synthesized by our group, following a similar approach.[9]

IR spectroscopy

The IR spectrum of $[RuCl_2(vpy)_4]$ differs slightly from that of free vpy,[17] with small shifts towards either longer or shorter wavenumbers, indicating that most of the vibrational modes have been preserved after coordination of vpy to the metallic center. Three bands have been identified for the complex at 925, 995 and 1630 cm^{-1}. The first two are sharp and intense, whereas the intensity of the third is rather low. Such bands are typical of substituent vinylic groups.[18] A band of medium intensity, typical of vinylic groups, was located at 1419 cm^{-1} and arises from a symmetric angular deformation taking place at the terminal methylene plane. The most prominent modifications observed consist of two bands at 640 and 426 cm^{-1}, corresponding to the coordinated pyridinic ring. Very similar bands in non-coordinated vpy were observed at 605 and 405 cm^{-1}, respectively. Similar shifts have been reported for *trans*-[$RuCl_2(py)_4$] by Clark and Williams,[19] as being rather sensitive to the symmetry of the complex. Such shifts have also been observed in other octahedral complexes.[20]

^{1}H and ^{13}C NMR of *trans*-[$RuCl_2(vpy)_4$]

Raichart and Taube[21] have demonstrated the use of ^{1}H NMR in the determination of the geometry (*cis* or *trans*) of complexes with general formula $[RuX_2L_4]$. The differentiation between the two geometries is based on the analysis of the protons nearest to the pyridinic N atom, as these species are quite sensitive to both the metallic center and axial halogens. Complexes having *trans* geometry show only one signal for pyridine protons attached to C^1 and C^5, whereas in *cis* geometry such protons give two signals in a 1:1 ratio. A similar argument can be applied to ^{13}C NMR spectra. Some discrepancy has been observed between the results obtained from ^{1}H and ^{13}C spectra for *trans*-[$RuCl_2(vpy)_4$] (Table 1). While ^{1}H analysis clearly indicated the *trans* geometry of the complex, the corresponding ^{13}C NMR spectrum were these results obtained in different work showed that C^1 and C^5, and C^2 and C^4, were inequivalent. Conversely, similar tests carried out in our facilities revealed the presence of only two single signals at δ 157.8 and 123.3, corresponding to protons attached to C^1/C^5, and C^2/C^4, respectively. Moreover, our synthesis from 'ruthenium blue' solutions has been successfully employed by several other groups[9–11,16] resulting in compounds with a *trans* geometry. Therefore, the results presented herein clearly suggest the existence of different environments resulting from a possible inclined radial conformation of the pyridinic rings around the metallic center.

Table 1 ^{1}H and ^{13}C NMR spectroscopic data for *trans*-[$RuCl_2(vpy)_4$] in $CDCl_3$

$\delta(^1H)$	assignment	$\delta(^{13}C)$	assignment
8.52	$2H^2$, H-Ar, dd, $J = 2.0$ and 7.6 Hz	160.2	C^1
7.30	$2H^3$, H-Ar, dd, $J = 1.5$ and 7.6 Hz	136.5	C^2
6.70	$1H^X$, $-CH=$, dd, $J = 11$ and 18 Hz	116.0	C^3
5.71	$1H^B$, $=CH_2$, dd, $J = 2$ and 11 Hz	133.4	C^4
5.69	$1H^A$, $=CH_2$, dd, $J = 2$ and 18 Hz	156.6	C^5
		122.7	C^6
		119.5	C^7

Electronic spectroscopy

The electronic spectrum of *trans*-[$RuCl_2(vpy)_4$] obtained in CH_2Cl_2 revealed the presence of a strong MLCT band at 446 nm and a weak shoulder at 500 nm whereas we observed a maximum absorption MLCT band at 398 nm in $CHCl_3$ for *trans*-[$RuCl_2(py)_4$], *i.e.* a red-shift of the bands of *ca.* 48 nm is seen from changing from L = py to vpy. The electronic spectrum of *trans*-[$RuCl_2(vpy)_4$] matches closely with that for *trans*-[$RuCl_2(pyca)_4$] (pyca = 4-pyridinecarboxylic acid), with a MLCT band at $\lambda_{max} = 464$ nm.[10] Thus, the spectral shift observed is most probably due to the presence of the substituent vinylic group at the 4 position of the pyridine ring.

Electrochemistry

The monomer in solution was studied in an attempt to correlate the redox properties of the monomer both in the free state and embedded in a polymeric matrix. Fig. 2 shows a typical cyclic voltammogram obtained at a scan rate of 100 mV s^{-1}. Data were obtained using a concentration of 5 mmol dm^{-3} of the monomer in a solution of CH_3CN–CH_2Cl_2 (9:1, v/v) with 0.10 mol dm^{-3} HTBA (tetrabutylammonium hexafluorophosphate). The redox process is metal-centered with E_{pa} at −61.19 mV attributed to the *trans*-$[RuCl_2(vpy)_4]^{0/+}$ process, whereas the reverse wave observed at E_{pc} −145.8 mV corresponds to the *trans*-$[RuCl_2(vpy)_4]^{+/0}$ process. This leads to $E_{1/2}$ of −103.5 mV *vs.* Ag–Ag^+, which differs slightly from the value reported by Mukaida and coworkers[11] for *trans*-[$RuCl_2(py)_4$], as well as that found in our earlier investigations. Similar values for $E_{1/2}$ were also obtained by us upon investigating other related complexes.[9,10] It should be pointed out that whereas the shifts of λ_{max} in the UV–VIS bands are highly dependent on the nature and

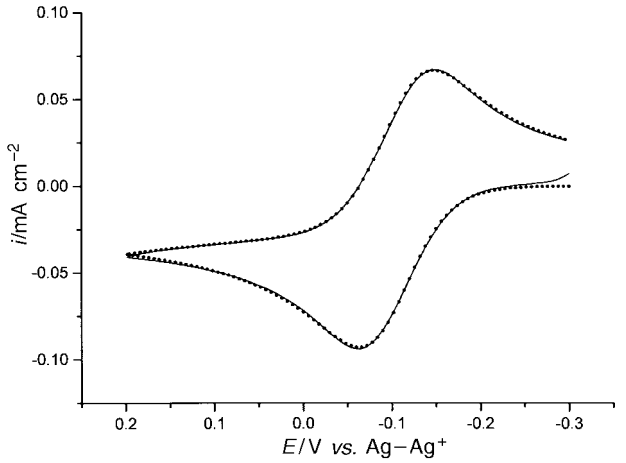

Fig. 2 Cyclic voltammogram obtained for the redox process of *trans*-$[RuCl_2(vpy)_4]$ (5×10^{-3} mol dm^{-3}) in CH_3CN–CH_2Cl_2 (9:1)–0.1 mol dm^{-3} HTBA (solid line) and simulated by COOL algorithm (dashed line)

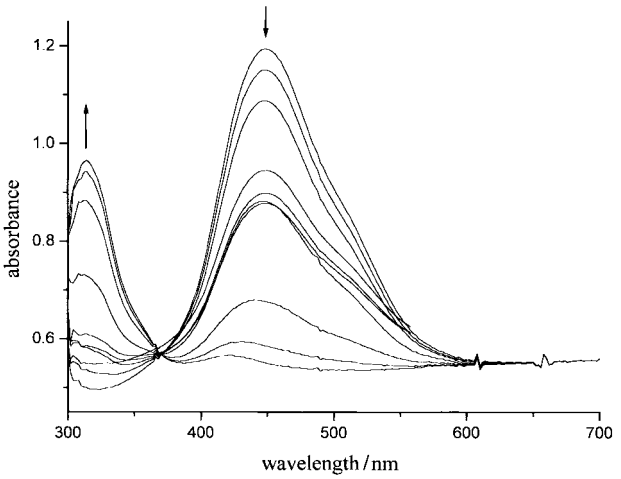

Fig. 3 Electronic spectrum of *trans*-$[RuCl_2(vpy)_4]$ oxidation in an OTTLE (ITO) obtained in the potential range from −0.30 to 0.30 V *vs.* Ag–Ag$^+$ in CH_3CN–CH_2Cl_2 (9:1v/v)–0.10 mol dm^{-3} HTBA

position of the substituent groups of the ligand, such an effect is not observed for $E_{1/2}$ since the redox process is metal-centered. A series of cyclic voltammograms obtained at various scan rates showed the linearity of i_{pa} *vs.* $v^{1/2}$ plots, which obey the Randles–Sevick equation. ΔE_p has a value of 84.61 mV after accounting for a 50 Ω *i*R drop. The full width at half height (FWHH) from differential pulse voltammetry is 100 mV, which is close to the theoretical value of 90 mV associated to a single electron process. The i_{pa}/i_{pc} ratio remains near unity for the entire scan rate investigated. Consecutive scans around the redox couple showed that the voltammetric profiles remained constant over time confirming the stability of the complex in solution. The experimental voltammograms showed a good correlation with that analyzed with the COOL algorithm[22] for a *quasi*reversible electrochemical mechanism. The same behavior was found by Paula and Franco for *trans*-$[RuCl_2(pmp)_4]$[9,13] as well as for novel pyridinic complexes of this family synthesized in our laboratory.[10]

Spectroelectrochemistry

Spectroelectrochemistry was carried out following the procedure described in a previous paper,[12] and was performed in the potential range between −0.30 and 0.30 V *vs.* Ag–$AgNO_3$. The characteristics of *trans*-$[RuCl_2(vpy)_4]$ were similar to those of related complexes synthesized in our laboratories.[9,10] The main band located at 446 nm disappeared upon oxidation of Ru^{II}, as shown in Fig. 3. Simultaneously, a new band arose at 310 nm, corresponding to the formation of Ru^{III}. The presence of an isosbestic point at 370 nm suggested the absence of any intermediate species between *trans*-$[RuCl_2(vpy)_4]^0$ and *trans*-$[RuCl_2(vpy)_4]^+$. At applied potentials lower than $E_{1/2}$, spectra corresponding to the reduced species were readily obtained. The system followed the Nernst equation with $E_{1/2}=-0.10$ V *vs.* Ag–Ag$^+$ obtained from a plot of E_{appl} *vs.* log([O]/[R]). The slope of the curve was approximately 59 mV, corresponding to a single electron redox process, which confirmed the value for the FWHH obtained by differential pulse voltammetry of 100 mV. The fact that the MLCT located at 446 nm faded and the development of a new band at 310 nm occurred during oxidation could also be observed by oxidative titration using aliquots of Br_2 in CH_2Cl_2. The resulting species in this case is likely also to be *trans*-$[RuCl_2(vpy)_4]^+$. The spectrum of the reduced species was readily re-established upon reduction with Zn amalgam in H_2SO_4.

Film growth by electropolymerization

It has been suggested that the polymerization of vinylpyridine can be anionically initiated.[23] Successive additions of monomers occur upon the generation of a carbanion which results in an anion with high molecular weight. At this point, it is essential that an aprotic polar solvent stabilizes the intermediate carbanion. Protic solvents are not recommended since any reaction that destroys the carbanion might also interrupt the electropolymerization. Thus a key aspect in successful electropolymerization lies in the choice of an appropriate solvent. Here, the binary CH_3CN–CH_2Cl_2 (4:1) system has been used in an attempt to satisfy the conditions of having both an aprotic solvent and one that will dissolve the monomer. Redox poly-*trans*-$[RuCl_2(vpy)_4]$ films were prepared using a variety of techniques and conditions. This work describes the results corresponding only to potentiostatic and galvanostatic electrodeposition. Results from cyclic voltammetric deposition, including data on the influence of the potential range, number of cycles, scan rate, as well as monomer concentration will be published at a later date.[24]

Potentiostatic growth

Films were potentiostatically grown on Pt, Pd, C glass and Au substrates in addition to sintered Fe–5%Ni and Fe–10%Ni substrates. The amount of material electrodeposited at a specific applied potential can be adjusted controlling either the deposition time or the material consumption on electroreduction. Following the electrodeposition, the electrodes were cleaned in an ultrasound acetone bath and transferred to a plain solvent/electrolyte cell (butan-2-one–0.1 mol dm^{-3} HTBA). The films were then electrochemically characterized by cyclic voltammetry. Fig. 4 shows the voltammetric profile of a film grown at an applied potential of −2.2 V under the conditions depicted in Fig. 3. The charge consumed was 50 mC. A potential scan carried out in the range −0.5 to 0.2 V indicated that the film was electroactive with $E_{1/2}{}^{surface}=-150.0$ mV, which corresponds to a shift of 50 mV towards cathodic values as compared to the monomer in solution. This suggests that the metallic center is not significantly affected by the electropolymerization. Previous studies[25–29] describing the preparation of redox films involving iron and ruthenium complexes containing ligands involving vinylic groups are in accord with these findings. The value of $E_{1/2}$ remained constant within a wide range of scan rates (20–7000 mV s^{-1}), whereas ΔE_p increased linearly with scan rate, with $\Delta E_p=30$ mV for a scan rate of 20 mV s^{-1}, but exceeding 204.0 mV for scan rates >200 mV s^{-1}. Such values of ΔE_p cannot be attributed solely to ohmic dropping effects, which are generally considerable and must be taken into account at high scan rates. However, in this case they should be rationalized in terms of the kinetics

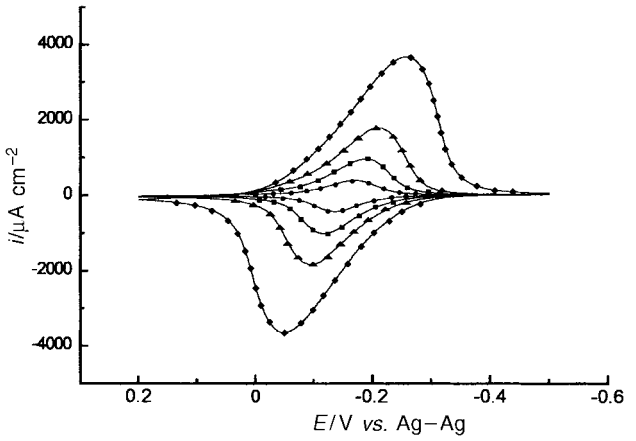

Fig. 4 Cyclic voltammogram of a potentiostatically film grown on a Pd electrode at −2.2 V. Consumption: 50 mC. butan-2-one–0.1 mol dm^{-3} HTBA. (●) 20 mV s^{-1}, (■) 50 mV s^{-1}, (▲) 100 mV s^{-1}, (◆) 250 mV s^{-1}.

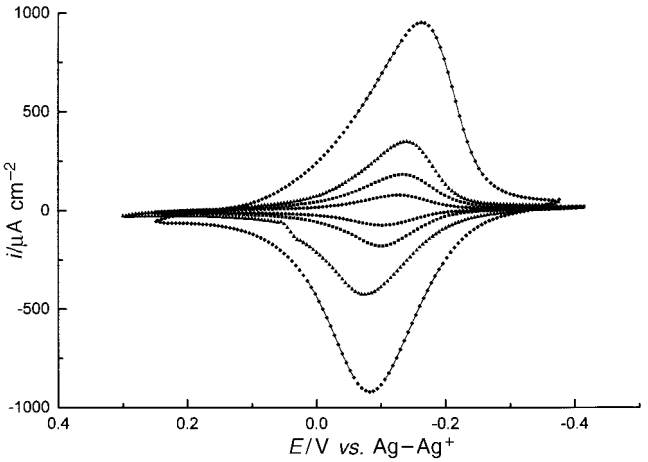

Fig. 5 Cyclic voltammogram of a galvanostatically film grown on a Pd electrode during 10 min. Current density: 4.3 mA cm^{-2}. Butan-2-one–0.1 mol dm^{-3} HTBA. (●) 50 mV s^{-1}, (■) 100 mV s^{-1}, (▲) 200 mV s^{-1}, (◆) 500 mV s^{-1}.

of electron transfer. Another possibility is that the peak separation is more likely to be due to slow ion transport in the film. In this sense, results from electrochemical impedance spectroscopy currently underway will clarify matters.

Differential pulse voltammetry suggested a value of FWHH of around 200 mV. The value of surface coverage Γ for the film, obtained from the integration of voltammetric waves was *ca.* 2.50×10^{-8} mol cm^{-2}, which corresponds to approximately 300 monolayers, according to the model proposed in the literature,[23] which considers a value of 8.3×10^{-11} mol cm^{-2} for a monolayer. Consecutive scans around $E_{1/2}$ for the metallic center showed that the electroactivity of the film remained unaffected even after >500 cycles. Several Pt and Pd electrodes were used to assess the redox properties in a solvent–electrolyte system containing ferrocene. The typical wave of the ferrocene–ferrocenium couple was essentially blocked. This confirmed the results from electronic microscopy analysis which suggested that the surface was uniformly coated. Upon polishing the electrode to remove the film, the voltammetric profile of the ferrocene wave is readily observed.

Galvanostatic growth

In addition to potentiostatic growth, films were also galvanostatically grown on a variety of electrodes including conventional electrodes, Pt and Pd sheets, and sintered Fe–5%Ni and Fe–10%Ni cylindrical electrodes. No growth was observed for current densities lower than 0.5 mA cm^{-2}, even for prolonged exposure periods (90 min). Current densities >5.0 mA cm^{-2} resulted in films with undesirable properties. The best results were achieved carrying out the electrodeposition in the range of 1.0–5.0 mA cm^{-2}. Fig. 5 depicts the voltammetric profiles obtained at various scan rates corresponding to a film galvanostatically grown on a Pd electrode at a current density of 4.3 mA cm^{-2}, during 10 min. Plots obtained at low scan rates featured a sinusoidal profile with $\Delta E_p = 20$ mV. Increasing the scan rate slightly deformed this profile. The value of $E_{1/2}$ obtained (−120 mV) was similar to that obtained for potentiostatically grown films. In general, the redox properties of films grown either potentiostatically or galvanostatically were similar, suggesting that the characteristics of the films have a more pronounced dependence on parameters such as type of solvent, concentration of electroactive species, potential, time, and current density, rather than nature of the electrode or deposition method. Fig. 6 shows a plot of $\log(i_{pa})$ *vs.* log(scan rate). The slope of the plot was calculated by linear fitting resulting in a value close to unity. Diffusion controlled processes usually feature slopes around 0.5. The coating rate was 1.7×10^{-9} mol cm^{-2} corresponding

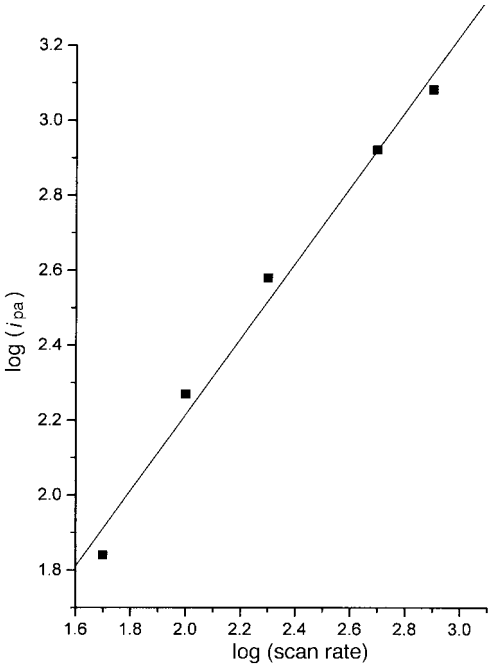

Fig. 6 Plot of $\log(i_{pa})$ *vs.* log(scan rate) corresponding to the film depicted in Fig. 5; (— — —) theoretical, (■) experimental

to 21 monolayers. A series of films was grown increasing the current density but keeping the time constant. The results showed that the slope of the curves decreased from 1 to about 0.5 with increasing coating rate, and consequently, with increasing current density. Such findings can be indicative of a thin multi-layer process taking place.

Electrodeposition on sintered electrodes

Films were electrodeposited on sintered Fe–5%Ni and Fe–10%Ni electrodes following an equivalent procedure as that used for inert electrodes. The properties of the resulting films were similar to those observed on inert electrodes. The microstructural analysis revealed that the morphology of the film was not significantly affected by the nature of the substrate (Fig. 7B and C). Electrochemical corrosion tests are presently underway to evaluate the efficiency of those films. The results of such tests will soon be published.

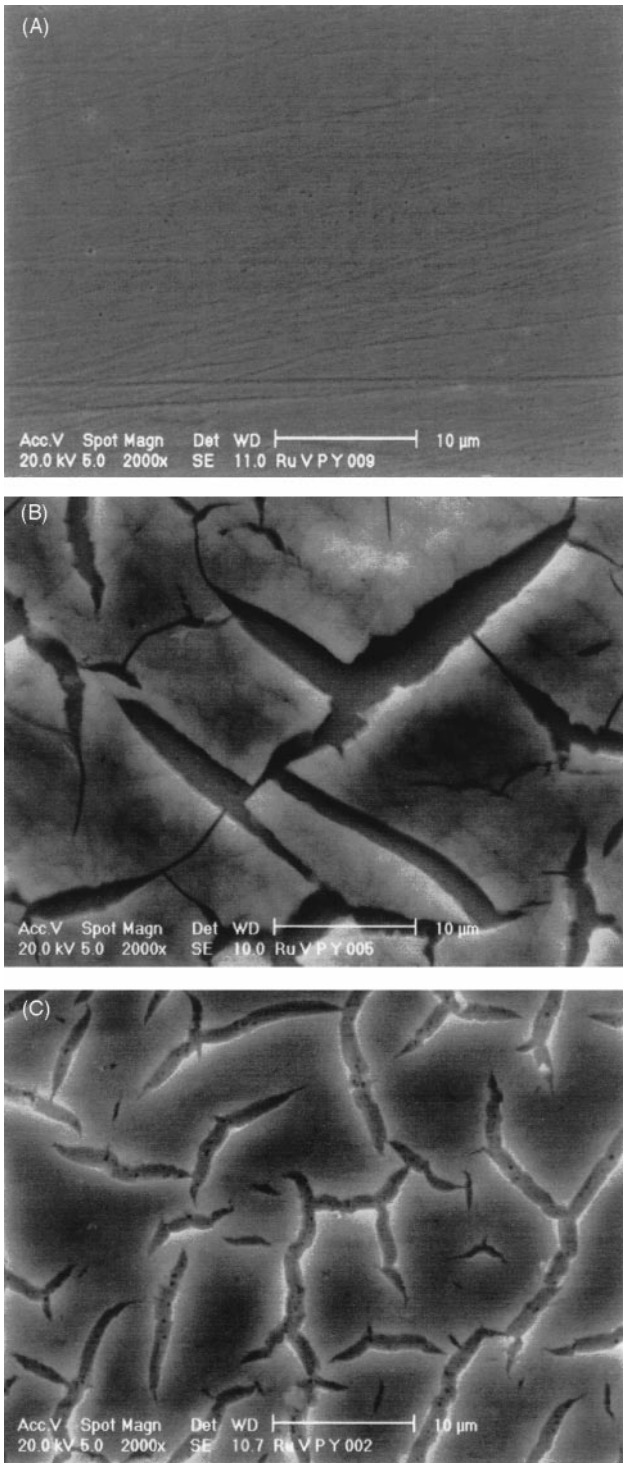

Fig. 7 (A) SEM image of Pt foil potentiostaticaly coated with poly-*trans*-$[RuCl_2(vpy)_4]$. (B) SEM image of poly-*trans*-$[RuCl_2(vpy)_4]$ film galvanostatically grown on a Fe–5%Ni electrode. Deposition time: 30 min. Current density: 2.3 mA cm^{-2}. (C) SEM image of poly-*trans*-$[RuCl_2(vpy)_4]$ film potentiostatically grown on a Fe–10%Ni electrode. Deposition time: 30 min. SEM parameters: acceleration voltage 20.0 kV, spot magnification 2000×.

Morphology

The film morphology appeared to be intimately related to layer thickness. Regardless of the nature of the substrate, thin films ($\Gamma \leqslant 5 \times 10^{-9}$ mol cm^{-2}) resulted in uniform coating characterized by a reddish metallic glitter (Fig. 7A). On the other hand, thicker films were usually red, opaque and brittle. Fig. 7B and C illustrate the microstructure of galvanostatically and potentiostatically grown films on Fe–5%Ni and Fe–10%Ni, revealing no significant difference in the appearance of the films. Although the micrographs show superficial cracking, EDS analyses carried out in the underlayer cracked region suggested uniform coating, indicating that cracking took place after a long deposition period. Thin films grown on Pt, Pd, and sintered electrodes showed uniform coating over the entire electrode surface. In addition, this films were also characterized by strong adherence. Fig. 8 shows the results of a EDS analysis carried out for the film depicted in Fig. 7A. A strong line could be seen at 2.7 keV corresponding to the presence of ruthenium, as was anticipated.

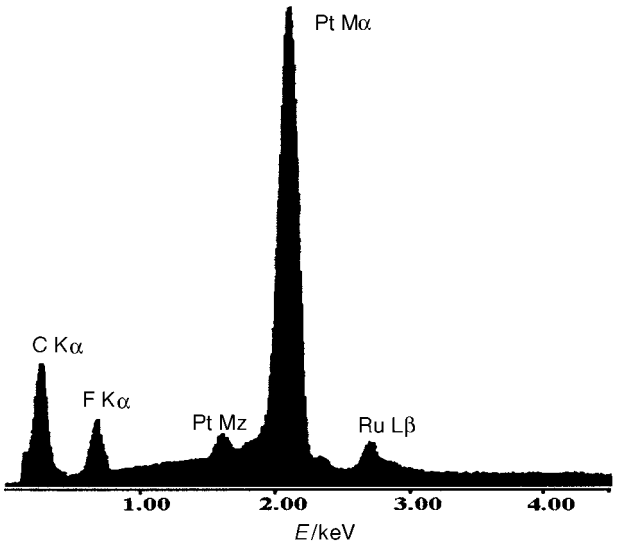

Fig. 8 EDS profile of the film depicted in Fig. 7(A)

Conclusions

The results showed herein demonstrate that the *trans*-$[RuCl_2(vpy)_4]$ monomer can be electrodeposited on the surface of inert as well as Fe (5–10%)Ni electrodes using both potential-controlled or current-controlled techniques. The redox properties of the resulting films were affected by the electrochemical parameters involved in the deposition process.

References

1 G. Troch-Nagels, R. Winand, A. Weymeersch and L. Renard, *J. Appl. Electrochem.*, 1992, **22**, 756.
2 F. Beck, *Electrochim. Acta*, 1988, **33**, 839.
3 A. De Bruyne, J. L. DelPlancke and R. Winand, *J. Appl. Electrochem.*, 1997, **27**, 867.
4 David W. DeBerry, *J. Electrochem. Soc.*, 1985, **132**, 1022.
5 F. Beck, R. Michaelis, F. Schloten and B. Zinger, *Electrochim. Acta*, 1994, **39**, 229.
6 F. Beck and R. Michaelis, *J. Coat. Technol.*, 1992, **64**, 59.
7 F. Beck and H. Guder, *J. Electrochem. Soc.*, 1987, **134**, 2416.
8 M. M. S. Paula and C. V. Franco, *J. Coord. Chem.*, 1995, **36**, 247.
9 M. M. S. Paula and C. V. Franco, *J. Coord. Chem.*, 1996, **40**, 71.
10 C. V. Franco, M. M. S. Paula, M. M. Meier and B. Szpoganicz, *J. Coord. Chem.*, in press.
11 H. Nagao, H. Nishimura, Y. Kitanaka, F. S. Howel, M. Mukaida and H. Kakihana, *Inorg. Chem.*, 1990, **29**, 1693.
12 M. M. S. Paula and C. V. Franco, *Quím. Nova*, 1994, **17**, 451.
13 C. V. Franco, M. M. S. Paula, P. Bodanese Prates and V. N. Moraes Jr., *Synth. Met.*, 1997, **90**, 81.
14 C. V. Franco, V. N. de Moraes Jr, F. Mocellin and M. M. S. Paula, unpublished work.
15 A. C. Boblitz Parente, A. V. C. Sobral, A. N. Klein, J. L. R. Muzart and C. V. Franco, *Adv. Powder Metall. Particulate Mater.*, 1996, **13**, 167.
16 J. D. Gilbert, D. Rose and G. Wilkinson, *J. Chem. Soc. A*, 1970, 2765.
17 C. J. Puchert, *The Aldrich Library of Infrared Spectra*, Aldrich Chemical, Milwaukee, 3rd edn., 1981.
18 R. M. Silverstein, G. C. Bassler and T. C. Morril, *Identificação*

Espectrométrica de Compostos Orgânicos (Portuguese Edition), ed. Guanabara Dois S. A., Rio de Janeiro, Brazil, 3rd edn., 1979.
19 R. J. H. Clark and G. S. Williams, *Inorg. Chem.*, 1965, **4**, 350.
20 R. J. H. Clark and G. S. Williams, *Chem. Ind.*, 1964, 3117.
21 D. W. Raichart and H. Taube, *Inorg. Chem.*, 1972, **11**, 999.
22 Model 271 COOL, Kinetic Analysis Software, User's Guide EG&G Instruments Corporation, 1992.
23 R. Kalir and A. Zilkha, *Eur. Polym. J.*, 1978, **14**, 557.
24 M. M. S. Paula and C. V. Franco, unpublished work.
25 T. F. Guarr and F. C. Anson, *J. Phys. Chem.*, 1987, **91**, 4037.
26 C. M. Elliott, C. J. Baldy, L. M. Nuwaysir and C. L. Wilkins, *Inorg. Chem.*, 1990, **29**, 389.
27 H. D. Abruña, P. Denisevich, M. Umaña, T. J. Meyer and R. W. Murray, *J. Am. Chem. Soc.*, 1981, **103**, 1.
28 P. Denisevich, H. D. Abruña, C. R. Leidner, T. J. Meyer and R. W. Murray, *Inorg. Chem.*, 1982, **21**, 2153.
29 P. G. Pickup, W. Kutner, C. R. Leidner and R. W. Murray, *J. Am. Chem. Soc.*, 1984, **106**, 1991.

Paper 8/02616E; *Received* 6*th April*, 1998